university of groningen

University Medical Center Groningen

University of Groningen

Modulating the water behavior, microstructure, and viscoelasticity of plasma-derived hydrogels by adding silica nanoparticles with tailored chemical and colloidal properties

Galeano-Duque, Y.; Sharma, P. K.; Mesa, M.

Published in:
Materials today communications

DOI:
10.1016/j.mtcomm.2022.105243

IMPORTANT NOTE: You are advised to consult the publisher's version (publisher's PDF) if you wish to cite from it. Please check the document version below.

Document Version
Publisher's PDF, also known as Version of record

Publication date:
2023

Link to publication in University of Groningen/UMCG research database

Citation for published version (APA):
Galeano-Duque, Y., Sharma, P. K., & Mesa, M. (2023). Modulating the water behavior, microstructure, and viscoelasticity of plasma-derived hydrogels by adding silica nanoparticles with tailored chemical and colloidal properties. *Materials today communications*, *34*, Article 105243. https://doi.org/10.1016/j.mtcomm.2022.105243

Copyright
Other than for strictly personal use, it is not permitted to download or to forward/distribute the text or part of it without the consent of the author(s) and/or copyright holder(s), unless the work is under an open content license (like Creative Commons).

The publication may also be distributed here under the terms of Article 25fa of the Dutch Copyright Act, indicated by the "Taverne" license. More information can be found on the University of Groningen website: https://www.rug.nl/library/open-access/self-archiving-pure/taverne-amendment.

Take-down policy
If you believe that this document breaches copyright please contact us providing details, and we will remove access to the work immediately and investigate your claim.

Downloaded from the University of Groningen/UMCG research database (Pure): http://www.rug.nl/research/portal. For technical reasons the number of authors shown on this cover page is limited to 10 maximum.

Materials Today Communications 34 (2023) 105243

Contents lists available at ScienceDirect

Materials Today Communications

journal homepage: www.elsevier.com/locate/mtcomm

Modulating the water behavior, microstructure, and viscoelasticity of plasma-derived hydrogels by adding silica nanoparticles with tailored chemical and colloidal properties

Y. Galeano-Duque [a], P.K. Sharma [b,c], M. Mesa [a,*]

[a] Materials Science Group, Institute of Chemistry, University of Antioquia, Calle 70 #52–21, AA 1226, Medellín 050010, Colombia
[b] University of Groningen, University Medical Center Groningen, W.J. Kolff Institute for Biomedical Engineering and Materials Science-FB41, A. Deusinglaan 1, 9713 AV Groningen, the Netherlands
[c] University of Groningen, University Medical Center Groningen, Department of Biomedical Engineering-FB40, A. Deusinglaan 1, 9713 AV Groningen, the Netherlands

ARTICLE INFO

Keywords:
Plasma
Hydrogels
Glycidoxypropyl-silica nanoparticles
Bound/free water
Viscoelasticity
Maxwell-Wiechert model

ABSTRACT

The viscoelastic properties of hydrogels depend on the tridimensional polymeric structure and the behavior of the liquid confined in their pores. The objective here is to modulate these characteristics in plasma-derived hydrogels by the addition of glycidoxypropyl-silica nanoparticles. These nanoparticles exhibited a hydrodynamic average size between 105.4 – 151.0 nm and surface coverage with (3-Glycidoxypropyl) trimethoxysilane of 0–96 %. The reinforced hydrogels are porous networks with spherical nanoparticles homogeneously distributed into their walls. The silanol groups of silica increase four-fold humidity retention compared with the native hydrogel. This correlates with bound water > 45 % on these reinforced hydrogels, in contrast with 75 % of free water on the native one (calculated from DSC in frozen hydrogels). The humidity stability can be also achieved in the hydrogel prepared with nanoparticles exhibiting 96 % organic coverage. Furthermore, this organic content promotes the microstructure chemical crosslinking, resulting in 3.9 and 1.6 higher Young's modulus compared with native and silica-reinforced hydrogels, respectively. The presence of glycidoxypropyl-silica nanoparticles in reinforced hydrogels modulated its viscoelasticity behavior, decreasing stress relaxation, which was explained using the generalized Maxwell-Wiechert model. In conclusion, novel organic-inorganic hybrid hydrogels based on plasma-derived ones and glycidoxypropyl-silica nanoparticles were developed. These nanoparticles are versatile and allow the production of hydrogels with improved viscoelastic behavior that also exhibits high water retention and morphological stability.

1. Introduction

Hydrogels are polymeric three-dimensional network structures, crosslinked physically and chemically. Hydrogels obtained from natural polymers including gelatin, alginate, cellulose, collagen, chitosan, and plasma [1–7] offer an advantage for biomedical applications over synthetic ones since they are inherently biocompatible, biodegradable, and easily recognized by tissues [8–10].

The hydrogels produced from blood plasma, bioinspired by the cloth biological roles [11–13]are highly appreciated for regenerative medicine and tissue engineering [14–19]. The cross-linking of protein fibers has been linked to both their stiffness and flexibility [14,20–22]. Furthermore, because of the hydrophilic nature of the proteins, these structures incorporate up to 99 % water, which results in a low protein cross-linking degree. This has an immediate effect on cell proliferation and mechanical properties, as it has been observed in many other biopolymer-based hydrogels [23–28].

The water confined in hydrogels can be classified according to how strongly it bonds to the polymeric network. The first type is the strong bound water. This interacts directly with the hydrophilic residues of the polymeric chains. The second type is the interstitial water which is trapped in the small pores of the hydrogel, surrounded by hydrophobic residues. The third type is the free, bulk, or excess water, stored in micropores without direct interaction with the polymer, therefore, exhibiting structure and thermal properties similar to pure liquid water [24,25,29]. The bound water affects the morphology, structure of hydrogels [24,26,27], and cell adhesion when they are used as cell scaffolds [27]. The water behavior present in the hydrogels network can be determined

* Corresponding author.
E-mail address: monica.mesa@udea.edu.co (M. Mesa).

https://doi.org/10.1016/j.mtcomm.2022.105243
Received 9 September 2022; Received in revised form 19 December 2022; Accepted 21 December 2022
Available online 28 December 2022
2352-4928/© 2022 Elsevier Ltd. All rights reserved.

by DSC, spectroscopic and computational techniques [24,25,28].

The high-water content suggests that the crosslinking and polymer amounts of hydrogels are low. This implies that they have low Young's modulus, low breaking points, and small elastic deformation limits. As a result, hydrogels easily break and cannot withstand high stresses[30]. The plasma and fibrin materials have been observed to present this behavior [13,14]. To improve these mechanical properties, composite hydrogels have been produced in the presence of fillers like silica nanoparticles[31–33]. As reported in the literature, Young's modulus measured by AFM for the hydrogel produced from human plasma was 1.5 kPa and increased to 8–10 kPa when Stöber silica nanoparticles (3 % w/v) were dispersed in the network [13]. These inorganic nanoparticles have tunable nanoscale size, mechanical stability, biodegradability, low toxicity, and versatility in surface chemical functionalization [34–40]. Organosilanes are efficient reagents to functionalize silica nanoparticles [41]. (3-Glycidoxypropyl) trimethoxysilane (GPTMS or GLYMO), is a very attractive functionalizer, due to it allows to obtain silica nanoparticles with rich surface chemistry by the presence of silanol, alkyl chains, epoxy, and/or diol groups [42]. GLYMO has an epoxide group that reacts with nucleophilic groups present in biopolymers leading to the formation of a covalent bond, while methoxy silane groups can be hydrolyzed to form silanol groups, and the latter condenses [43] to build a network of siloxanes, achieving the crosslinking of the biopolymers [44,45].

Hydrogels can be described as viscoelastic materials. If they are subjected to deformations, there is a mechanical response associated with their elasticity in which energy is stored and viscous contribution in which energy is dissipated. The combination of the elastic and viscous response leads to a time-dependent stress dissipation, known as the relaxation process [46]. Changes in the viscoelastic behavior of hydrogels reinforced with silica nanoparticles can be modeled using the generalized Maxwell-Wiechert model. In this model relaxation of polymer fibers occurs at different times, depending on their length, structure, water strength bond, and cross-linking degree [47].

The novelty of this paper relies on the possibility of mediating the water-protein interactions through the glycidoxypropyl-silica nanoparticles with tailored chemical and colloidal properties. They give new opportunities to modulate the mechanical behavior of the plasma-derived hydrogels, which lose a pronounced amount of water when they are manipulated [48]. The addition of silica to these plasma gels was also reported, but they needed to use glutaraldehyde for protein crosslinking and mechanical improvement [49]. Nude silica nanoparticles increased 1.5 times Young's modulus of alginate-polyacrylamide gels [50] and GLYMO was used for producing chitosan–organosilane hybrid materials with improved viscoelastic properties [51]. However, the use of glycidoxypropyl-silica nanoparticles, with organic-inorganic dual reactivity, for reinforcing plasma hydrogels has not been reported up to date. In the current work, the effect of glycidoxypropyl-silica on the microstructure, water behavior, and viscoelasticity of the reinforced hydrogels was evaluated and compared with plasma-derived native ones. The tailoring of silica chemistry and colloid characteristics by covalent grafting of (3-Glycidoxypropyl) trimethoxysilane is shown by microscopic, colloidal, thermal, and spectroscopic analysis. This ensures their high dispersion on plasma and homogeneous incorporation into the hydrogel network. Then, hydrogels were characterized in terms of microscopic structure, dehydration kinetic, water bonding, stress relaxation tests, Young's modulus determination, and viscoelastic modeling using the generalized Maxwell-Wiechert model of the hydrogels. Finally, the properties of plasma-derived hydrogel were correlated with the physicochemical characteristics of glycidoxypropyl-silica nanoparticles.

2. Materials and methods

2.1. Materials

Ethanol (CH_3CH_2OH > 99 % J. T. Baker), Ammonium hydroxide (30 % NH_4OH, AppliChem), Tetraethyl orthosilicate (98 % TEOS, Merck), (3-Glycidyloxypropyl) trimethoxysilane (GLYMO >98 % Sigma Aldrich). Human plasma donated by the Blood bank of the Alma Mater Hospital in Medellín-Colombia. Saline solution (0.9 % NaCl, Corpaul). Tranexamic acid commercial presentation (Knovel Pharma). Calcium Chloride (1 % $CaCl_2$ Sigma Aldrich). Ultrapure type 1 water, Mili-Q (Synergy® UV).

2.2. Synthesis of silica particles and functionalization with GLYMO

Unfunctionalized silica nanoparticles (S Nps) were prepared using a modified Stöber method [35]. In brief, 1.66 mmol TEOS were dropwise added to H_2O: CH_3CH_2OH: NH_4OH solution with a volume ratio of 3.40: 100: 3.78. The system was subjected to an ultrasound probe (1 min, pulse-on 10 s, pulse-off 5 s, and 90 % output). It was left under magnetic stirring at 350 rpm for 24 h, at 25 °C in a closed container to avoid the volatilization of ammonia. S Nps were washed by centrifugation/redispersion four times with water (Mili-Q grade).

The fresh S Nps were resuspended on ethanol (10 mL) and the GLYMO was added with a nominal concentration of 0.1 %, 0.5 %, and 1.0 % (v/v). The functionalized glycidoxypropyl-silica Nps were labeled as G0.1, G0.5, and G1, respectively. These systems were refluxed at 80 °C, under magnetic stirring at 250 rpm, for 24 h. They were washed by centrifugation/redispersion four times with acetone and water (Mili-Q grade). The Nps before and after functionalization were characterized by Dynamic Light Scattering (DLS), ζ-potential, Thermogravimetric Analysis (TGA), N_2 adsorption-desorption isotherms, ^{29}Si Solid-state Nuclear Magnetic Resonance (^{29}Si CP-MAS NMR), X-ray Photoelectron Spectroscopy (XPS) and Scanning Electron Microscopy (SEM) for comparing their physicochemical properties.

2.2.1. Particle size, ζ-potential, and morphology

S Nps and glycidoxypropyl-silica Nps size distributions based on intensity were determined by Dynamic Light Scattering (DLS) using Horiba LB 550 equipment. The measurements were carried out at 25 °C in an aqueous dispersion at pH 7. The polydispersity index (PDI) was calculated by Eq. 1 from the hydrodynamic average size and standard deviation (SDT) of the peak.

$$\mathrm{PDI} = \left(\frac{\mathrm{SDT}}{\mathrm{mean}}\right)^2 \quad (1)$$

The values were interpreted as highly monodisperse (PDI < 0.05), homogeneous narrow distribution (PDI < 0.2–0.3), and highly polydisperse (PDI > 0.7) [52].

The ζ-potential was determined at pH 7 for all Nps dispersed in water, by using a Malvern Zetasizer Nano Z instrument. The morphology of dried Nps was evaluated by SEM in the JSM-6490LV microscope (JEOL). The samples were dispersed in ethanol, deposited on graphite tape, and coated with gold (Denton vacuum Desk IV) to enhance the electric conductivity. The Energy Dispersive spectroscopy (EDS) analysis was performed for determining the silicon and carbon distribution on the particles.

2.2.2. Specific surface area

The N_2 adsorption-desorption isotherms, at 77 K, were measured in Micromeritics ASAP 2020 for the S and glycidoxypropyl-silica (G0.1, G0.5, and G1). Samples were activated at 100 °C for 12 h under a vacuum. The specific surface area (B in m^2/g) was calculated with the equipment software from the BET model.

2.2.3. Moisture and GLYMO coverage of nanoparticles surface

The moisture and organic content of glycidoxypropyl-silica Nps were determined through thermogravimetric analysis (TGA) in a Q500 TGA equipment (TA Instruments). The samples were heated under air at 10 °C/min from 30 °C to 800 °C. The weight loss below 100 °C was reported as the moisture percentage. The thermal event under 100 °C was taken to calculate the moisture percentage of Nps and the thermal event between 200 °C and 300 °C was taken for calculation of the attached GLYMO. This gave the organic fraction (δ) regarding the net dried weight of the material and then, GLYMO grafting density (μmol ligand/m^2 of NPs surface, ∅) was calculated by Eq. 2.

$$\varnothing = \frac{\delta}{(1-\delta)BM} * 10^6 \quad (2)$$

where B (specific surface area of Nps m^2/g); M is the molecular weight of the pendant organic chain on the Nps surface that is removable during the heating (133 g/mol). The surface coverage percentage of functionalized Nps was calculated by dividing ∅ by 7.6 μmol grafted ligand/m^2. This value corresponds to 100 % monolayer coverage on the Nps surface, assuming 4.6 SiOH groups per nm^2 as available grafting sites[53].

2.2.4. Chemical functionalization

The covalent grafting of Nps with (3-Glycidoxypropyl) trimethoxysilane (GLYMO) on the Nps surface was confirmed by ^{29}Si CP-MAS NMR, on a Bruker Advance III equipment at 9.4 T, under Harmanm-Hann conditions. The chemical environment on the functionalized Nps was characterized by X-ray photoelectronic spectroscopy (XPS). The survey and high-resolution spectra were obtained using a monochromatized Al Kα x-ray source (1486.7 eV, 13 kV, 100 W). The spectra were taken in contact analyzer energy (CAE) mode using 100 eV pass energy for the survey and 30 eV for high-resolution acquisition. Kα charge compensation system is employed with an energy of 10 eV. The C1s peak attributed to C-(C-H) at a binding energy of 284.8 eV is a signal of adventitious carbon and it is used as a reference for the binding energy calibration.

2.3. Preparation and characterization of plasma-derived hydrogels

The plasma-derived hydrogels were prepared according to the protocol described by Gaviria et al. [54], by mixing human plasma (67 % v/v), normal saline solution (18 % v/v), tranexamic acid (1.4 % v/v), and different concentrations of Nps (0–4 mg/mL). The gelation was induced by the addition of 1 % $CaCl_2$ solution (14 % v/v) and aging for 30 min at 37 °C. The hydrogels obtained were named PS, PG0.1, PG0.5, and PG1, according to the Nps type added. The native plasma-derived hydrogels (P) were prepared in the absence of siliceous Nps. The microstructure, dehydration kinetic, water behavior, and viscoelastic properties of hydrogels were evaluated through different techniques described below.

2.3.1. Microstructure

The wet hydrogels were analyzed by SEM in the JSM-6490LV microscope (JEOL), with a low vacuum, and cooling the samples at − 25 °C with the COOLSTAGE SEM device. This procedure was used to minimize changes in hydrogel structure due to water evaporation. For comparative purposes, some hydrogel samples were lyophilized under standard conditions at − 89 °C and high vacuum (0.8 mbar) before SEM analysis.

2.3.2. Dehydration kinetics

The plasma-derived hydrogels were left in an open container under atmospheric conditions, to follow spontaneous drying. The humidity retention was determined gravimetrically (Eq. 3), registering the mass change of each hydrogel upon drying at room temperature for 168 h (7 days).

$$\text{Dehydration}(\%) = \left(\frac{W_0 - W_i}{W_0 - W_p}\right) * 100 \quad (3)$$

where W_0, W_i, and W_p were the weights (mg) of the wet hydrogel at zero time (i.e. fully hydrated), different times of drying, and fully dry after 7 days, respectively.

2.3.3. Water behavior

The Differential Scanning Calorimetry (DSC) measurements were performed using Q100 (TA Instruments) to analyze the water trapped in the pores of the hydrogels. The following heating program was used: cooling to − 50 °C at 10 °C/min with a 5 min isotherm before heating up to 150 °C at 5 °C/min. A linear baseline was used for integrating peaks to determine the enthalpies of melting (ΔH_m) of water. TA instruments universal analysis 2000 Software was used. Bound water was calculated by Eq. 4, taking the melting enthalpy of pure water as a reference ($\Delta H_m(\text{ref}) = 333.55 J/g$).

$$\text{Bound water}(\%) = \left[1 - \left(\frac{\Delta H_m(i)}{\Delta H_m(\text{ref})}\right)\right] * 100 \quad (4)$$

Were $\Delta H_m(i)$ is the water melting enthalpy found for plasma suspension, native (P), and reinforced hydrogels (PS, PG0.1, PG0.5, and PG1).

2.3.4. Viscoelastic properties by stress relaxation tests

The hydrogels were subjected to a stress relaxation test under uniaxial compression using a Low-Load Compression Tester (LLCT) at 25 °C as described previously [55–58]. The LabVIEW 7.1 program was used for LLCT load cell and linear positioning for control and data acquisition. Native and reinforced hydrogels (2 and 4 mg/mL of S and G1 Nps) were deformed by 20 % of their original thickness (strain $\varepsilon = 0.2$) at a deformation speed of 20 %/s (strain rate $\dot{\varepsilon} = 0.2 s^{-1}$). The diameter of the indentation probe was 2.5 mm diameter. The deformation was held constant for 60 s and the changes in stress were monitored. In the compression test, the stress vs strain curve was plotted, and a linear increase in stress as a function of strain was observed between a strain of 0.04 and 0.1; the slope of the line fit to this region was taken as Young's modulus. Due to Young's modulus of the viscoelastic hydrogels changing with the strain rate, the values reported here are valid only at a strain rate of 0.2 s^{-1}.

On the stress relaxation measures, the required stress to maintain a constant strain of 20 %, continuously decreases with time, which is a clear indication of the viscoelastic nature of protein-based hydrogels. The stress relaxation curve was mathematically modeled with a generalized Maxwell- Wiechert model. The relaxing stress as a function of time [σ(t)] was divided by the constant strain of 0.2 to obtain the value of continuously decreasing modulus E(t). Data were acquired using Eq. 5 which describes the generalized Maxwell-Wiechert model. Then the values of the spring constant (E_i) and the relaxation time constant (τ_i) for individual Maxwell elements (where i varies from 1 to n) were calculated. The generalized model is composed of various Maxwell elements connected in parallel, each element represents a spring indicating the elastic response to unloading and a dashpot accounting for the viscous response[58] (SI Fig. S1a). Each element is characterized by a relaxation time constant (τ_i), i.e., the time scale over which the element is significant. The number of Maxwell elements necessary to fit the experimental data was determined by visually fitting a plot that shows the decrease in χ^2value with the addition of every extra Maxwell element (SI Fig. S1b). The required number of Maxwell elements was chosen when no further decrease in χ^2 was observed (SI Fig. S1b).

$$E(t) = E_1 e^{-t/\tau_1} + E_2 e^{-t/\tau_2} + E_3 e^{-t/\tau_3} + \ldots + E_n e^{-t/\tau_n} \quad (5)$$

The relative importance (R_i) of each Maxwell element in terms of percentage within the relaxation process was expressed as the proportion of its spring constant (E_i) to the sum of all spring constants used, and

it was calculated using Eq. 6.

$$R_i = 100 * \frac{E_i}{\sum_{i=1}^{n} E_i} \quad (6)$$

2.4. Statistical analysis

All sample preparation and analysis were made in triplicate. Comparisons for more than two groups were done using one-way ANOVA with Tukey's post hoc test. A *p-value < 0.05 was considered statistically significant. Results are expressed as mean ± standard error of the mean.

3. Results and discussion

3.1. Glycidoxypropyl-silica nanoparticles

The unfunctionalized S Nps, synthetized in this work by the modified Stöber method [34,35], have spherical morphology. The particle size distribution measured by DLS in water at pH 7 is monomodal and monodisperse (PDI: 0.08) with an average size of 105.4 ± 4.0 nm, which agrees with the size determined by SEM after drying (Fig. 1a). The S Nps have a negative ζ-potential of − 44.4 ± 0.8 mV (Fig. 1a), due to the presence of deprotonated silanol groups on the surface at pH 7. This favors the interparticle electrostatic repulsion and therefore, explains the monodisperse nature and colloidal stability of this dispersion [59].

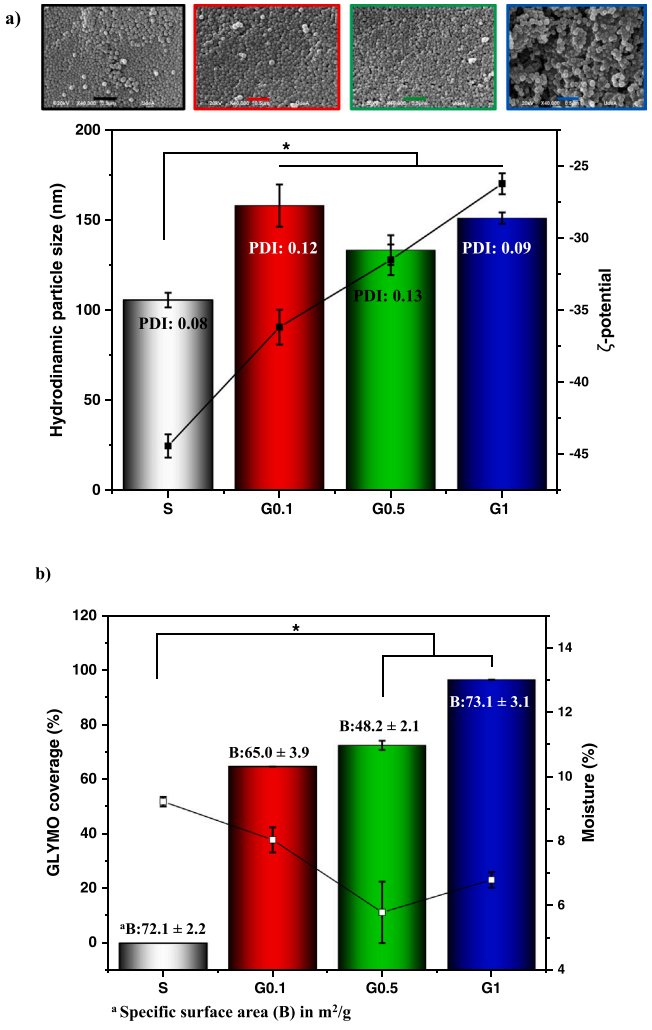

Fig. 1. Colloidal and surface characterization of unfunctionalized (S) and glycidoxypropyl-silica (G0.1, G0.5, G1) nanoparticles. (a) Hydrodynamic particle size (bar), ζ-potential (line) at pH 7 in aqueous dispersion, and SEM micrographs. Significance difference, $p < 0.05$ (*), was calculated for hydrodynamic particle size and ζ-potential. (b) Surface coverage with GLYMO (bar) and moisture % (line) from TGA thermograms. Significance difference, $p < 0.05$ (*), was calculated for moisture %.

A small increase in the particle average size is measured after functionalization with 0.1–1.0 % v/v GLYMO (DLS and SEM), as a consequence of the hydrodynamic length of the glycidoxypropyl pendant chains, without affecting the spherical morphology (Fig. 1a). The interparticle condensation under the functionalization conditions could also contribute to the size increase by agglomeration [59]. Therefore, the used GLYMO was limited up to 1.0 % v/v to avoid extensive GLYMO self-condensation and particle aggregation. The functionalization of the glycidoxypropyl-silica surface through silanol condensation makes less negative the ζ-potential of these Nps (Fig. 1a) [43]. Some silanol groups are still on the non-fully GLYMO-covered surface contributing to the negative surface. The glycidodypropyl-silica coverage increases in function of the initial GLYMO concentration from 64 % to 96 % (Fig. 1b), without affecting the monodispersity (Fig. 1a). This high dispersion is due to the combined contributions of steric and electrostatic stabilization[60], through glycidoxypropyl pendant chains and charged silanols of the surface, respectively.

The monolayer coverage percentage of glycidoxypropyl-silica Nps affects their water adsorption capacity. There is an inverse relationship between GLYMO coverage on the surface and moisture percentage, except for G1 Nps (Fig. 1b). The unfunctionalized S Nps exhibit the highest moisture percentage favored by the highest specific surface area (Fig. 1b). The presence of the silanol groups also contributes to the increase of moisture percentage, due to particles promoting water interaction by H-bonds. For G0.1 and G0.5 Nps, the presence of alkyl chains and lower specific surface areadecreases the water interactions. However, when the coverage reaches 96 % on G1 Nps, there is not a significant change in the moisture respecting G0.5 Nps. On the contrary, the tendency is to increase water adsorption, which can be related to the high surface area of this G1 material and the chemistry of the surface. The oxygenated terminal groups of pendant chains on glycidoxypropyl-silica Nps should contribute to H-bonds, dipole-dipole, and Van der Waals interactions with water. Additionally, the probability of new silanol groups coming from dioxane and polyether secondary products [61] is not discarded due to the higher GLYMO quantity, which contributes to rising affinity with water. These physicochemical characteristics also explain the nanoparticle dispersibility in water, even with the highest GLYMO coverage (Fig. 1a,b).

The chemistry of the surface was explored from ^{29}Si CP-MAS NMR and XPS results. The covalent grafting of GLYMO, by condensation with the silanol on the silica surface [43], was demonstrated by the apparition of T_3 and T_2 signals on the typical ^{29}Si CP-MAS NMR spectrum of functionalized Nps (Fig. 2a). These are related to the Si-C bond [62,63]. The Q_2 and Q_3 signals, ascribed to Si on geminal and single silanol groups, are still present on functionalized Nps as a result of the non-full coverage with GLYMO. The XPS analysis gives more information about the chemical environment of organic terminal groups on the surface (Fig. 2b,c). The general XPS spectra glycidoxypropyl-silica materials exhibit signals for Si2p (103.8 eV) and O1s (533.1 eV) accompanied by C1s around 285.6 eV (Fig. 2b). The O/Si ratio near to 2 corresponds to the theoretical value for siliceous materials [64]. The high-resolution C1s spectrum for G1 Nps allows identifying C adventitious (284.8 eV), C-(C, H) (286.3 eV), and C-O (287.9 eV) signals, related to ether and epoxy in GLYMO pendant chains [65].

According to the preceding results, the surface of the glycidoxypropyl-silica nanoparticles can be described as in Fig. 2d, where the negative charge could come from non-attached silanols and the alkyl chain can be epoxy and diol terminated. The surface characteristics and their effects on the water adsorption and dispersibility, enable these nanoparticles to be suspended homogeneously on the aqueous plasma acting as reinforcement fillers of plasma-derived

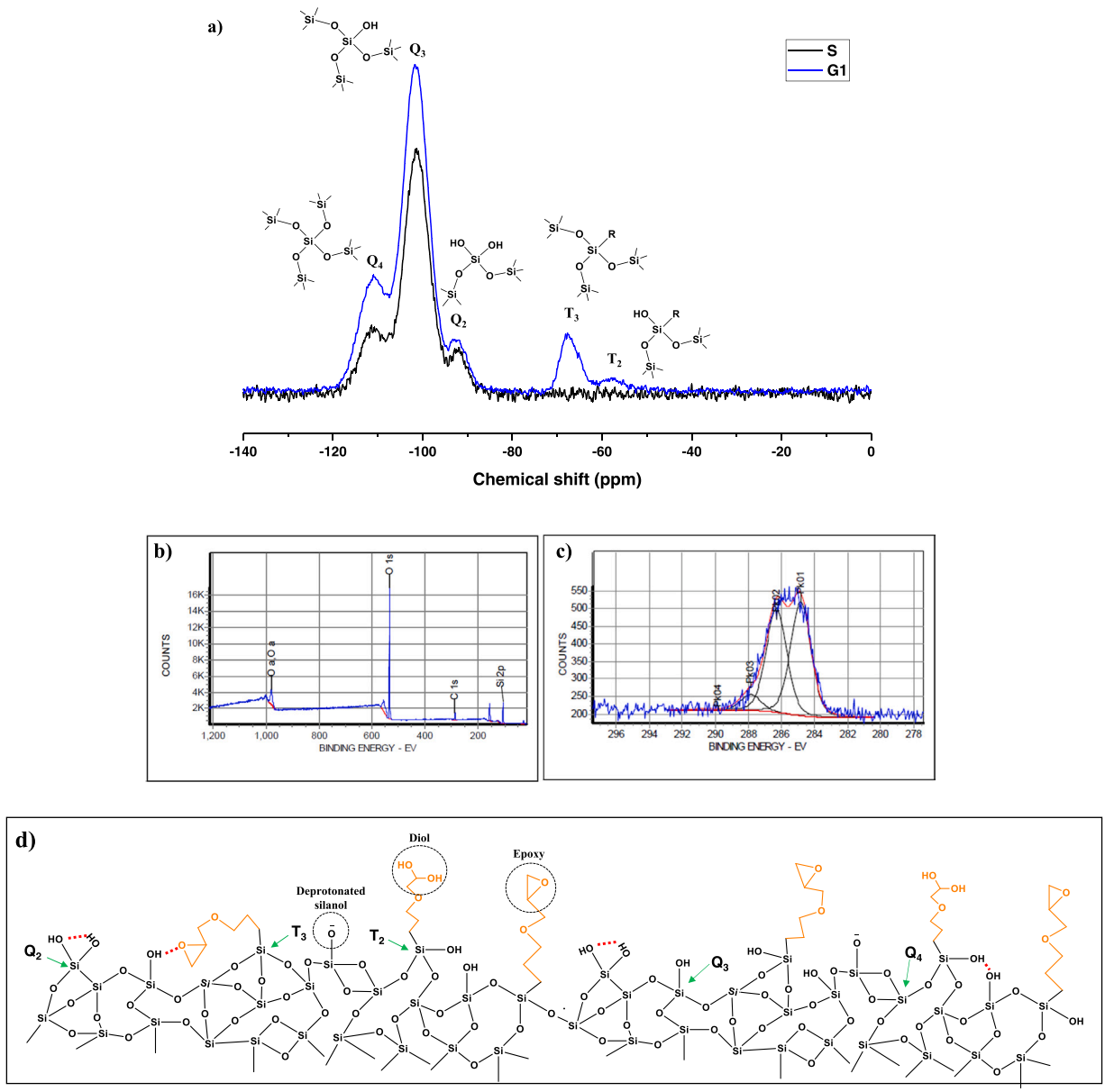

Fig. 2. (a) Chemical characterization of unfunctionalized S and glycidoxypropyl-silica (G0.1, G0.5, G1) nanoparticles by ^{29}Si CP-MAS NMR. (b) General XPS. (c) C1s high-resolution XPS. (d) Surface chemistry model.

hydrogels.

3.2. *Characterization of the hydrogels microstructure and water behavior*

The native and reinforced hydrogels of this work are produced from human blood plasma through in vitro gelation initiated by $CaCl_2$ [12], in the absence and presence of silica (S) or glycidoxypropyl-silica Nps (G0.1, G0.5, and G1). The characteristics of the hydrogels microstructure and water behavior on their pores are determined by SEM, gravimetry, and DSC.

The native hydrogel exhibits a microstructure of interconnected pores, with sizes between 7 and 35 μm (Fig. 3a). This is also observed in the reinforced hydrogels, where the siliceous spherical Nps behave like nodes between the fibers, and they are incorporated into the walls of the hydrogel pores (Fig. 3b-d). Probably, the unfunctionalized S and glycidoxypropyl-silica Nps induce the hydrogel gelation around them, acting as nucleation agents through multiple electrostatic, dipole-dipole, and H-bond interactions [66]. Moreover, the reaction of epoxy groups with nucleophilic residues of proteins can promote the chemical crosslinking of the hydrogel. The siliceous materials are uniformly distributed along with the gel structure, as evidenced on the EDS compositional maps (Fig. 3h), contributing to the homogeneous microstructure of reinforced hydrogels. This demonstrates the effective interaction of these nanoparticles with fibrinogen and other plasma proteins during the gelation process, due to the excellent dispersibility (Fig. 1a) on aqueous media. In addition, the particle size of both S, and glycidoxypropyl-silica Nps (Fig. 1a), allows the obtention of homogeneous hybrid hydrogels without phase segregation. The porosity of the hydrogel structure was preserved after its reinforcement with glycidoxypropyl-silica nanoparticles. The nanoscale size of the siliceous materials prevents the clogging of hydrogel pores, which will have an impact on key hydrogel properties such as swelling capacity. Also, it is important to maintain the porosity of the hydrogels because it has been reported, in biomedical applications, that open and interconnected pores are necessary for fast cell colonization or drug release [67].

The presence of S or glycidoxypropyl-silica Nps on reinforced materials avoids the total collapse of the 3D porous microstructure of the native hydrogel during drying by lyophilization (Fig. 3e-g). This means

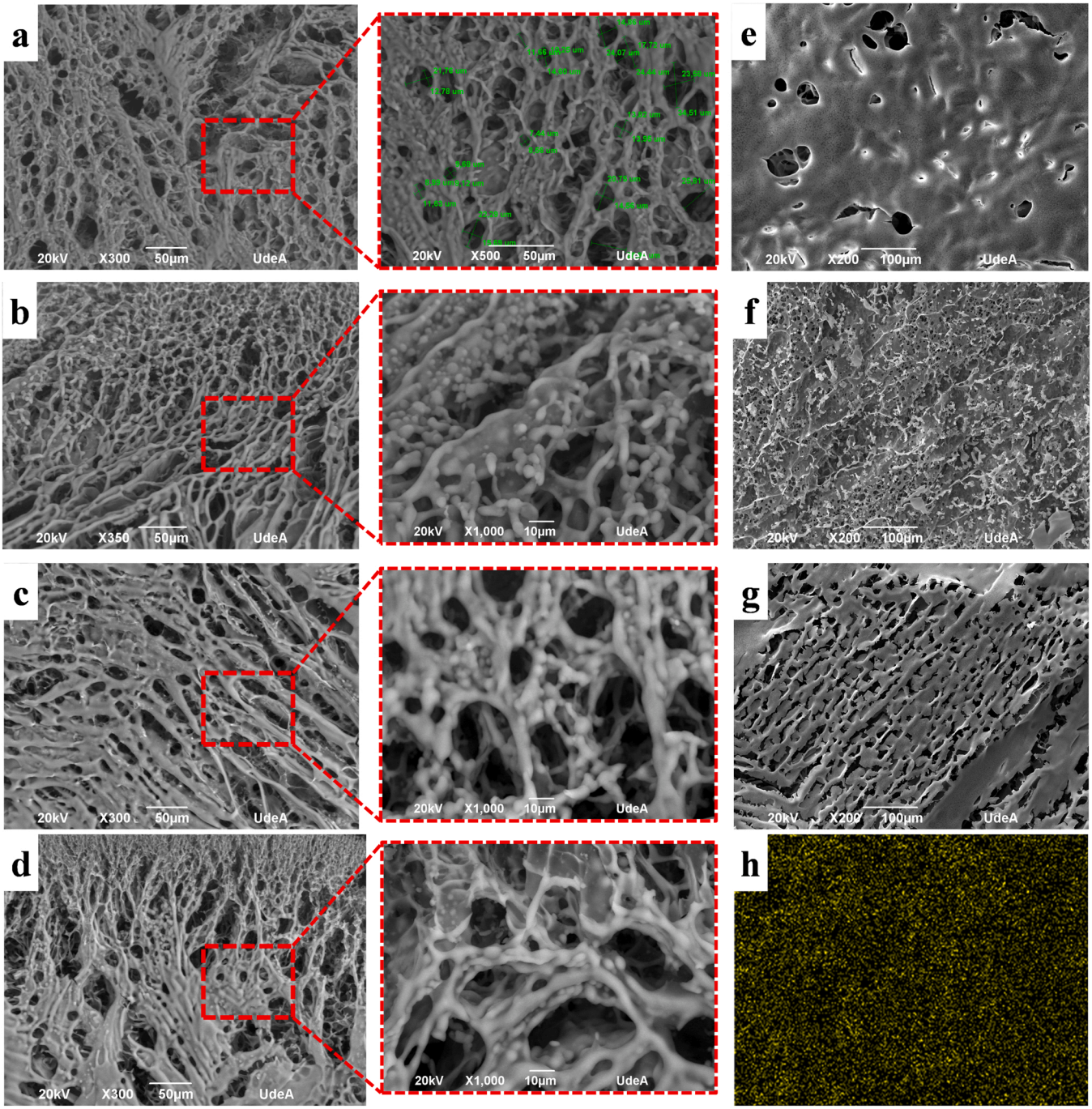

Fig. 3. SEM micrographs at − 25 °C for wet samples (a-d) and room temperature for lyophilized ones (e-g): native P hydrogel (a,e) PS (b,f), PG0.1 (c,g) and PG0.5 (d) (reinforced 4 mg/mL of Nps). The silicon map from Energy Dispersive spectroscopy (EDS) for PS sample (h).

that particles minimize the stress caused by water solidification and sublimation during the freeze-drying (lyophilization) process of hydrogels. However, it is highly advisable to keep the wet hydrogels, for preserving the microstructure and humidity, which are important for their functionality in future applications as cell scaffolds and wound dressings [48,55].

Based on these results, the microstructure of reinforced hydrogels can be described as a hybrid organic-inorganic network, in which the water entrapment and stability of their porous structures are mediated by siliceous materials. This is corroborated quantitatively by the dehydration kinetics of the hydrogels at room temperature and the study of the water behavior from DSC analysis. The dehydration is slower and lower for the reinforced hydrogels than for the native P one (Fig. 4a). Mainly, the PS hydrogels reinforced with unfunctionalized S Nps can maintain the humidity, in direct correlation with the high capability of these particles for adsorbing water (expressed as moisture %) through silanol groups in their high surface area (Fig. 1b). The DSC analysis of wet samples after freezing at − 21 °C gives additional information about the molecular interactions of water inside the hydrogel network. The two endothermic events in the DSC thermogram correspond to water melting and vaporization (Fig. 4b). These temperatures and the corresponding enthalpies are shifted from the values for the bulk water, as a result of their confinement into the porous hydrogel [18,28]. In this environment, some molecules are adsorbed on the pore walls and others are in the inner part, mainly in interaction with themselves (Fig. 4d). Then, the classification as bound and free water, respectively, has been

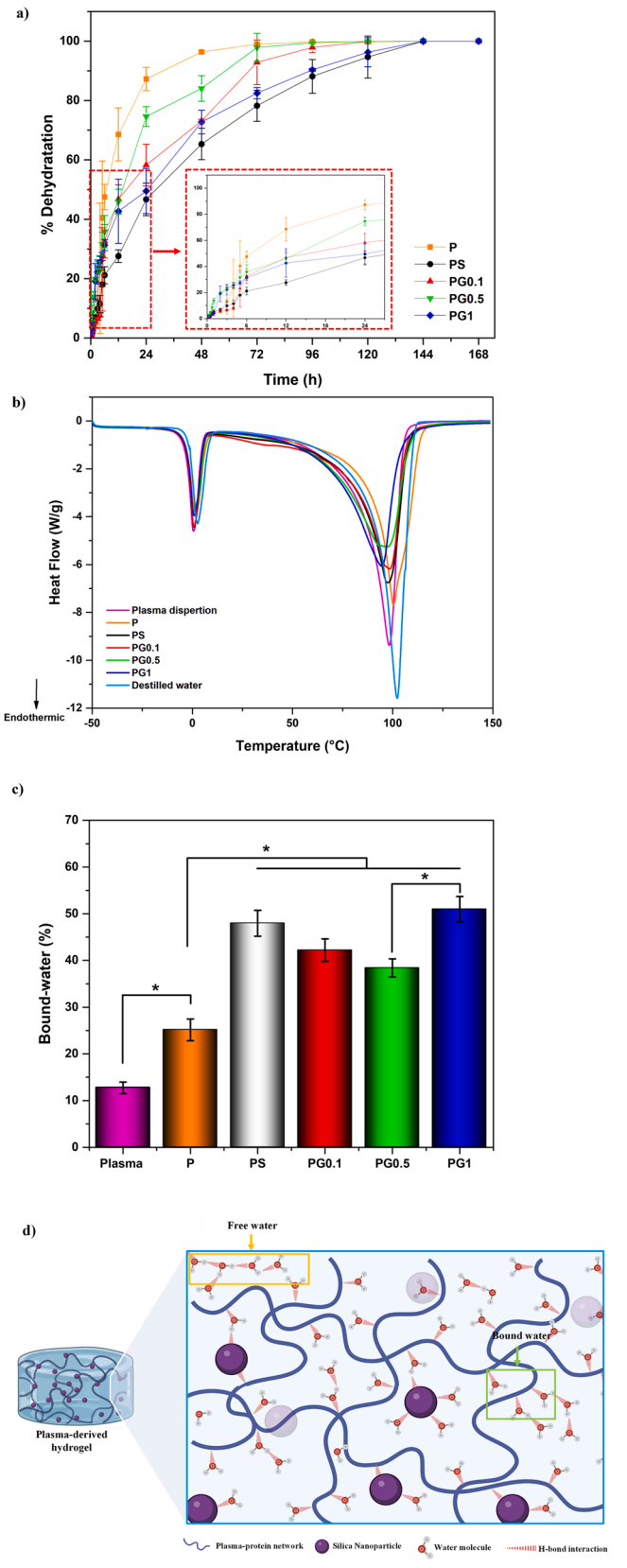

Fig. 4. (a) Dehydration kinetic curve at room temperature. (b) Differential Scanning Calorimetry (DSC) thermograms. (c) Bound water calculated by Eq. 4 from DSC to native (P) and reinforced (4 mg/mL) hydrogels (PS, PG0.1, PG0.5, and PG1). Significance difference, $p < 0.05$ (*), was calculated for bound-water (%). (d) Scheme of free and bound water entrapped into the porous structure.

adopted [24,25]. Considering that bound water is the main responsible for the decrease in the melting enthalpy, this value can be used for the calculation of bound water percentage (Eq. 4). In fact, the water can be also bound to plasma proteins but its entrapment on the hydrogels network increases this percentage. Moreover, the presence of silica and glycidoxypropyl-silica Nps on the tridimensional structure of reinforced hydrogels causes an additional increment of the bound water (Fig. 4d). It is interesting to notice the similarity between this tendency and the moisture % of Nps (Fig. 1b). The silanol groups on the unfunctionalized silica S Nps improve the water interaction inside the hydrogel and therefore, its entrapment and retention into the PS hydrogels. The G0.5 Nps, which exhibit the lower specific surface area and water adsorption ability, contribute to a lesser extent to the percentage of bound water in the PG0.5 reinforced hydrogel and its stability during the dehydration experiment (Fig. 4a). Additionally, the epoxy groups of the G0.5 Nps are involved in chemical crosslinking, which reduces the diol formation and their interaction with water into the hydrogels. In the case of the PG1 hydrogels, the bound water and dehydration extent comes out comparable with those in PS hydrogels. It is because the 96 % surface coverage with organic GLYMO on G1 is quite high for contributing to network chemical crosslinking and still having hydrophilic groups for favoring the water interactions mediated by nanoparticles in the microstructure. For blood plasma and whey soy protein gels with pore sizes in the range of 0.2–2 μm, it has been reported they lose a pronounced amount of water when they are manipulated [48]. However, the reinforced plasma-derived hydrogel with glycidoxypropyl-silica can hold large percentages of bound water which is related to slow dehydration kinetics (Fig. 4a).

3.3. Viscoelastic properties of reinforced hydrogels

The native P hydrogels are highly extensible (Fig. 5a). Based on the literature, this hydrogel can stretch up to three times its length before breaking and twice its length without permanent distortion [20–22]. However, it loses a large amount of water (Fig. 4a), especially when it is subjected to deformation. This can lead to damage to its tridimensional structure during handling since the mechanical properties of hydrogels depend on the network microstructure and the liquid confined into the porous [68]. The reinforced hydrogels preserve the stretchability of the native hydrogel, with improved resistance to breaking, as it is shown qualitatively in the photos (Fig. 5c-e). Considering that PS and PG1 materials, reinforced with 4 mg/mL Nps, exhibit higher stability against the water lost, in direct correlation with the higher percentages of bound water on the network (Fig. 4a,c), they were selected for studying the viscoelastic properties in function of the surface chemistry of the Nps incorporated on their walls. Some comparisons will be made with hydrogels reinforced with 2 mg/mL of Nps. These samples will be identified with a number 2 in parenthesis.

The stress relaxation assay revealed that the maximum stress applied to reach 20 % deformation of the reinforced hydrogels is higher compared to natives in the following order: PG1(4) > PS(4) >PG1 (2) > PS(2) > P. This indicates the stiffness was improved by the presence of siliceous materials, especially on the hydrogel reinforced with 4 mg/mL of G1 Nps. At longer times, the relaxation process or stress decay takes place. It involves the release of internal energy, due to the polymer chains rearranging to take the energetically most favorable position with the lowest entropy [69]. The relaxation occurs to a greater extent in native P hydrogels than in PS and PG1 ones. In PS the chains are easily rearranged, plastic deformations occur, and the flow of the hydrogel predominates. For PG1, it is observed that this relaxation process is slower because the interactions with glycidoxypropyl-silica nanoparticles lead to a slightly slower relaxation of the chains. Furthermore, it was found that PG1(4) with glycidoxypropyl-silica concentration at 4 mg/mL, it is feasible to create a hydrogel with a lower relaxation compared to the other hydrogels. This behavior is caused by the synergistic effect of particle concentration increase and particle-protein

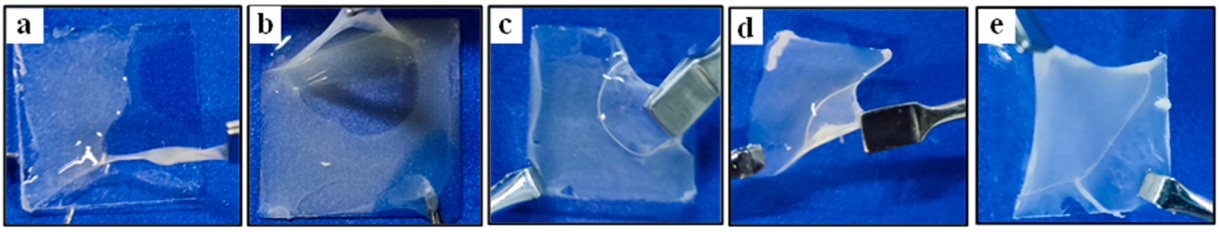

Fig. 5. Representative photographs for (a) native P. (b) PS. (c) PG0.1. (d) PG0.5. (e) PG1. Silica and glycidoxypropyl-silica concentration was 4 mg/mL.

covalent interaction promotion.

The decrease in the relaxation of hydrogel reinforced with nanoparticles can be associated with the increase in stiffness represented by Young's modulus (Fig. 6b). The calculated Young's modulus using the linear stress-strain curve showed an increase as follows: PG1(4) > PS(4) > PG1(2) > PS(2) > P. The most significant differences with the native P hydrogel are seen when the Nps concentration was 4 mg/mL (Fig. 6b). This is because the hydrogel-free volume is reduced as the Nps concentration is raised, which in turn restricts the movement of the protein chains on the polymeric network. Additionally, the use of functionalized glycidoxypropyl-silica promotes the formation of covalent bonds in the hydrogel walls, improving the mechanical stability, especially on PG1 (4) hydrogels. This result agrees with the increase in the percentage of glycidoxy coverage (Fig. 1b). By increasing the percentage of glycidoxy groups exposed on the surface of the nanoparticle, the formation of covalent bonds between the particle and the protein network is promoted, which leads to having more rigid and mechanically stable materials. This, together with the high-water retention, helps the preservation of the hydrogel network integrity during the deformation experiment.

Viscoelastic stress relaxation is caused by several events taking place at the molecular level, such as changes in protein bonds or the movement of water molecules within the hydrogel porous network. The Maxwell-Wiechert model allows dividing the total relaxation data into Maxwell elements which can be theoretically attributed to the physical components of the hydrogel. These changes can be reflected in the relaxation time constants and the relative importance of the particular Maxwell element, predicted by Maxwell-Wiechert model.

Native hydrogels (P) require two Maxwell elements to explain the relaxation profile while reinforced hydrogels (PS, PG1) require three elements, except for PG1(2) which requires four elements (Fig. 6c). The Maxwell element 1 is associated with those components of the hydrogel that easily dissipate energy, such as water, which flows relatively quickly through the pores and channels of the deformed hydrogel. This

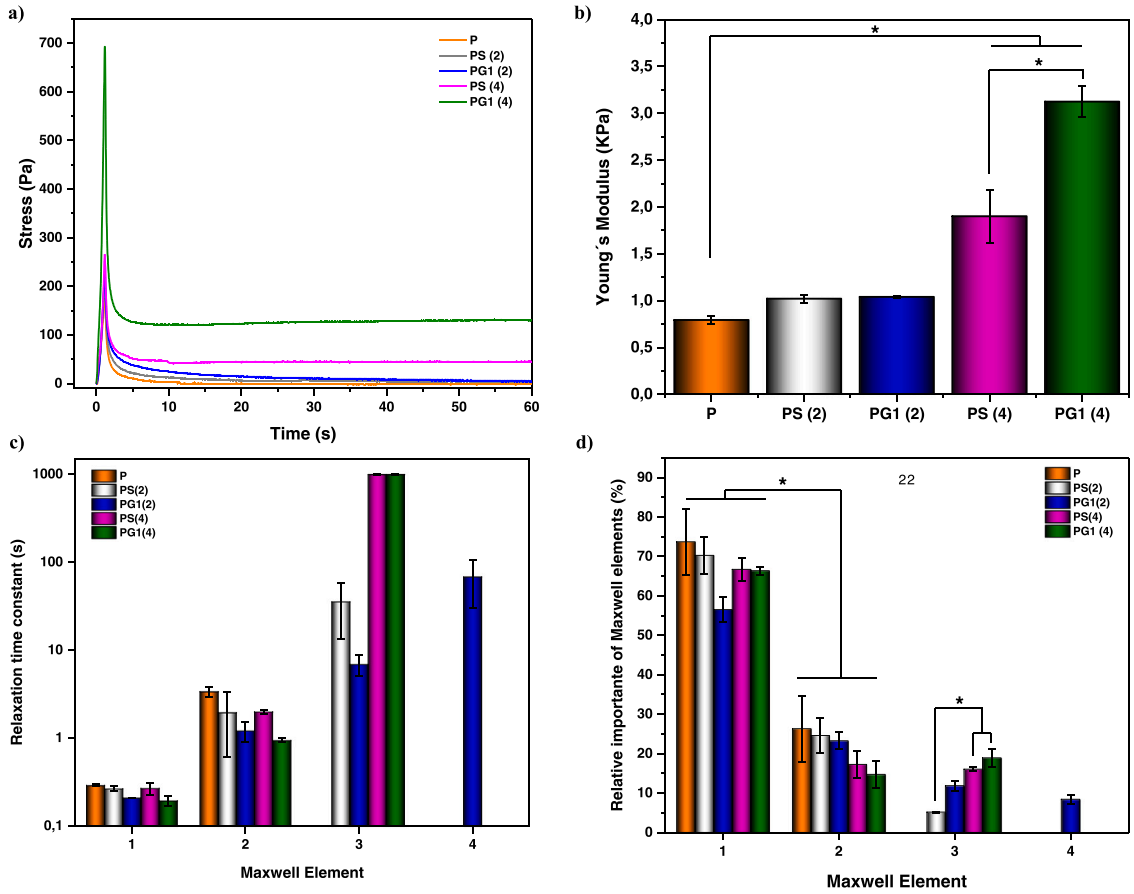

Fig. 6. Viscoelastic properties studied from stress-relaxation. (a) Stress-time curves with a constant strain of 20 % and strain rate of 0.2 s^{-1}. (b) Calculated Young's modulus from the elastic zone at 0.04–0.1 strain. (c) Relaxation time constant (s) for each Maxwell element, using the generalized Maxwell-Wiechert model. (d) Relative importance (%) of each Maxwell element for native hydrogel (P), reinforced plasma hydrogel, PS(2), and PS(4) with 2 and 4 mg/mL of S Nps, respectively. PG1(2) and PG1(4) with 2 and 4 mg/mL glycidoxypropyl-silica G1, respectively.

is the element with the highest relative importance for native hydrogel P. For reinforced hydrogels, it is observed a decrease in the relative importance of Maxwell elements 1 and 2, (τ_1: fast and τ_2: intermediate elements) [70] and increase in the relative importance of element 3 (τ_3 : slow element). According to Maxwell-Wiechert model, the addition of elements to explain the relaxation process on reinforced hydrogels implies that the relaxation of these is more complex compared with native hydrogels. These changes are due to the interactions generated between the polymeric network and the silica or glycidoxypropyl-silica Nps (Fig. 6c). These findings are consistent with those obtained from dehydration kinetics (Fig. 4a) and DSC (Fig. 4c), which show that native hydrogels lose more water and have a smaller percentage of bound water than reinforced hydrogels.

The PG1 showed a greater extent of relative importance for Maxwell element 3 (R_3: 18.9 ± 2 %) and a relaxation time constant τ_3: 900 s (Fig. 6d), which is associated with slower relaxation processes. These results agree with the increase in hydrogel stiffness reported by Young's modulus. (Fig. 6b).

4. Conclusion

Functionalization of monodispersed silica nanoparticles with 3-Glycidyloxypropyl trimethoxy silane effectively conferred electrostatic-steric colloidal stability and tailored chemical reactivity. Then, they can be homogeneously distributed throughout the plasma hydrogel without phase separations. Their surface silanols and glycidoxypropyl chemical groups allowed for higher water retention on reinforced hydrogels than in the native ones, contributing to the slower dehydration kinetic. The bound water participated in the hydrogel network structure and extensibility preservation by H-bonds, dipole-dipole, and electrostatic interactions. Moreover, the favorable interactions between the silica nanoparticles and the protein network decrease the relaxation of polymeric chains, modulating the viscoelastic behavior of these hydrogels.

These results indicate that glycidoxypropyl-silica are great candidates to balance the stiffness/elasticity of these plasma-derived hydrogels, by controlling the water retention ability and mechanical stability. These are critical aspects to apply this kind of biomaterials as wound dressings.

CRediT authorship contribution statement

Y. Galeano-Duque: Conceptualization, Methodology, Investigation, Data curation, Visualization, Formal analysis, Writing – original draft preparation, Writing – review & editing. **P. K. Sharma:** Supervision, Resources, Software, Validation, Writing – review & editing. **M. Mesa:** Conceptualization, Supervision, Resources, Software, Validation, Formal analysis, Writing – review & editing.

Declaration of Competing Interest

The authors declare that they have no known competing financial interests or personal relationships that could have appeared to influence the work reported in this paper.

Data Availability

Data will be made available on request.

Acknowledgments

The authors thank the scholarship awarded by the Abel Tasman Talent Program of the Faculty of Medical Sciences at University Medical Center Groningen in Groningen-The Netherlands.

Statement of significance

Plasma-derived hydrogels, mechanically reinforced with silica, exhibiting stable tridimensional microstructure and water confined in their pores, are designed in this work. Tailored chemical surfaces of glycidoxypropyl-silica nanoparticles improve the humidity retention and morphological/mechanical stability of hydrogels, through physical and chemical crosslinking, as shown by thermodynamic and spectroscopic techniques. Theoretical modeling of the viscoelastic results using the Maxwell-Wiechert model shows the complex and improved viscoelastic behavior of these hydrogels. They exhibited 3.9 higher Young's modulus and 20 times lower stress relaxation when subjected to compressive deformations compared to the native plasma-derived ones, in conjunction with the strongest bonded water. These characteristics are crucial for enabling the performance of these biomaterials as wound dressings and cell scaffolds in future applications.

Appendix A. Supporting information

Supplementary data associated with this article can be found in the online version at doi:10.1016/j.mtcomm.2022.105243.

References

[1] D. Boso, E. Carraro, E. Maghin, S. Todros, A. Dedja, M. Giomo, N. Elvassore, P. de Coppi, P.G. Pavan, M. Piccoli, Porcine decellularized diaphragm hydrogel: a new option for skeletal muscle malformations, Biomedicines 9 (2021) 709, https://doi.org/10.3390/biomedicines9070709.
[2] S.K. Park, J.H. Shin, J.H. Jung, D.Y. Lee, D.Y. Choi, S.H. Yoo, Polysaccharide-derivative coated intravascular catheters with superior multifunctional performance via simple and biocompatible method, Chem. Eng. J. 433 (2022), 134565, https://doi.org/10.1016/j.cej.2022.134565.
[3] X. Shi, D. Cantu-Crouch, V. Sharma, J. Pruitt, G. Yao, K. Fukazawa, J.Y. Wu, K. Ishihara, Surface characterization of a silicone hydrogel contact lens having bioinspired 2-methacryloyloxyethyl phosphorylcholine polymer layer in hydrated state, Colloids Surf. B Biointerfaces 199 (2021), 111539, https://doi.org/10.1016/j.colsurfb.2020.111539.
[4] K.M. Salleh, S. Zakaria, M.S. Sajab, S. Gan, H. Kaco, Superabsorbent hydrogel from oil palm empty fruit bunch cellulose and sodium carboxymethylcellulose, Int J. Biol. Macromol. 131 (2019) 50–59, https://doi.org/10.1016/j.ijbiomac.2019.03.028.
[5] T. Distler, A.R. Boccaccini, 3D printing of electrically conductive hydrogels for tissue engineering and biosensors-a review, Acta Biomater. 101 (2020) 1–13, https://doi.org/10.1016/j.actbio.2019.08.044.
[6] V.K. Pal, R. Jain, S. Sen, K. Kailasam, S. Roy, Designing nanofibrillar cellulose peptide conjugated polymeric hydrogel scaffold for controlling cellular behavior, Cellulose 28 (2021) 10335–10357, https://doi.org/10.1007/s10570-021-04176-z.
[7] R.C. Op't Veld, X.F. Walboomers, J.A. Jansen, F.A.D.T.G. Wagener, Design considerations for hydrogel wound dressings: strategic and molecular advances, Tissue Eng. Part B Rev. 26 (2020) 230–248, https://doi.org/10.1089/ten.teb.2019.0281.
[8] M. Klein, E. Poverenov, Natural biopolymer-based hydrogels for use in food and agriculture, J. Sci. Food Agric. 100 (2020) 2337–2347, https://doi.org/10.1002/jsfa.10274.
[9] A. Mahmood, D. Patel, B. Hickson, J. Desrochers, X. Hu, Recent progress in biopolymer-based hydrogel materials for biomedical applications, Int J. Mol. Sci. 23 (2022) 1415, https://doi.org/10.3390/ijms23031415.
[10] N. Martin, G. Youssef, Dynamic properties of hydrogels and fiber-reinforced hydrogels, J. Mech. Behav. Biomed. Mater. 85 (2018) 194–200, https://doi.org/10.1016/j.jmbbm.2018.06.008.
[11] E. Anitua, P. Nurden, R. Prado, A.T. Nurden, S. Padilla, Autologous fibrin scaffolds: when platelet and plasma derived biomolecules meet fibrin, Biomaterials 192 (2019) 440–460, https://doi.org/10.1016/j.biomaterials.2018.11.029.
[12] S. Natesan, R. Stone, R.E. Coronado, N.L. Wrice, A.C. Kowalczewski, D.O. Zamora, R.J. Christy, PEGylated platelet-free blood plasma-based hydrogels for full-thickness wound regeneration, Adv. Wound Care (N. Rochelle) 8 (2019) 323–340, https://doi.org/10.1089/wound.2018.0844.
[13] N.Y. Becerra, L.M. Restrepo, Y. Galeano, A.C. Tobón, L.F. Turizo, M. Mesa, Improving fibrin hydrogels' mechanical properties, through addition of silica or chitosan-silica materials, for potential application as wound dressings, Int J. Biomater. 2021 (2021) 1–11, https://doi.org/10.1155/2021/9933331.
[14] K.C. Murphy, J. Whitehead, D. Zhou, S.S. Ho, J.K. Leach, Engineering fibrin hydrogels to promote the wound healing potential of mesenchymal stem cell spheroids, Acta Biomater. 64 (2017) 176–186, https://doi.org/10.1016/j.actbio.2017.10.007.
[15] A.K. Gaharwar, N.A. Peppas, A. Khademhosseini, Nanocomposite hydrogels for biomedical applications, Biotechnol. Bioeng. 111 (2014) 441–453, https://doi.org/10.1002/bit.25160.

[16] P. Heher, S. Mühleder, R. Mittermayr, H. Redl, P. Slezak, Fibrin-based delivery strategies for acute and chronic wound healing, Adv. Drug Deliv. Rev. 129 (2018) 134–147, https://doi.org/10.1016/j.addr.2017.12.007.
[17] R. Tanaka, Y. Saito, Y. Fujiwara, J. ichiro Jo, Y. Tabata, Preparation of fibrin hydrogels to promote the recruitment of anti-inflammatory macrophages, Acta Biomater. 89 (2019) 152–165, https://doi.org/10.1016/j.actbio.2019.03.011.
[18] S.E. Noorjahan, T.P. Sastry, Hydrogels based on physiologically clotted fibrin-gelatin composites, J. Polym. Sci. A Polym. Chem. 42 (2004) 2241–2252, https://doi.org/10.1002/pola.20055.
[19] R.I. Litvinov, J.W. Weisel, Fibrin mechanical properties and their structural origins, Matrix Biol. 60 (2017) 110–123, https://doi.org/10.1016/j.matbio.2016.08.003.
[20] C.C. Helms, R.A.S. Ariëns, S. Uitte De Willige, K.F. Standeven, M. Guthold, α-α Cross-links increase fibrin fiber elasticity and stiffness, Biophys. J. 102 (2012) 168–175, https://doi.org/10.1016/j.bpj.2011.11.4016.
[21] W. Liu, L.M. Jawerth, E.A. Sparks, M.R. Falvo, R.R. Hantgan, R. Superfine, S. T. Lord, M. Guthold, Fibrin fibers have extraordinary extensibility and elasticity, Science 313 (2006) (1979) 634, https://doi.org/10.1126/science.1127317.
[22] W. Liu, C.R. Carlisle, E.A. Sparks, M. Guthold, The mechanical properties of single fibrin fibers, J. Thromb. Haemost. 8 (2010) 1030–1036, https://doi.org/10.1111/j.1538-7836.2010.03745.x.
[23] L. Zhu, X. Zhang, Z. Shao, M. Guo, Highly stretchable, compressible, resilient, and equilibrium swelling hydrogels with elastic nano junctions, Macromol. Mater. Eng. 305 (2020) 2000205, https://doi.org/10.1002/mame.202000205.
[24] K. Piechocki, M. Kozanecki, J. Saramak, Water structure and hydration of polymer network in PMEO2MA hydrogels, Polymer 210 (2020), 122974, https://doi.org/10.1016/j.polymer.2020.122974.
[25] V.M. Gun'ko, I.N. Savina, S. v Mikhalovsky, Properties of water bound in hydrogels, Gels 3 (2017) 37, https://doi.org/10.3390/gels3040037.
[26] N. Buchtová, A.D. Orlando, P. Judeinstein, O. Chauvet, P. Weiss, J. le Bideau, Water dynamics in silanized hydroxypropyl methylcellulose based hydrogels designed for tissue engineering, Carbohydr. Polym. 202 (2018) 404–408, https://doi.org/10.1016/j.carbpol.2018.08.143.
[27] K. Numata, T. Katashima, T. Sakai, State of water, molecular structure, and cytotoxicity of silk hydrogels, Biomacromolecules 12 (2011) 2137–2144, https://doi.org/10.1021/bm200221u.
[28] C. Yan, P.L. Kramer, R. Yuan, M.D. Fayer, Water dynamics in polyacrylamide hydrogels, J. Am. Chem. Soc. 140 (2018) 9466–9477, https://doi.org/10.1021/jacs.8b03547.
[29] H. Yoshida, T. Hatakeyama, H. Hatakeyama, Characterization of water in polysaccharide hydrogels by DSC, J. Therm. Anal. Calor. 40 (1993) 483–489, https://doi.org/10.1007/BF02546617.
[30] A.R. Karimi, B. Rostaminejad, L. Rahimi, A. Khodadadi, H. Khanmohammadi, A. Shahriari, Chitosan hydrogels cross-linked with tris(2-(2-formylphenoxy)ethyl) amine: Swelling and drug delivery, Int J. Biol. Macromol. 118 (2018) 1863–1870, https://doi.org/10.1016/j.ijbiomac.2018.07.037.
[31] K. Wang, K. Albert, G. Mosser, B. Haye, A. Percot, C. Paris, C. Peccate, L. Trichet, T. Coradin, Self-assembly/condensation interplay in nano-to-microfibrillar silicified fibrin hydrogels, Int J. Biol. Macromol. 164 (2020) 1422–1431, https://doi.org/10.1016/j.ijbiomac.2020.07.220.
[32] S. Björkegren, L. Nordstierna, A. Törncrona, A. Palmqvist, Hydrophilic and hydrophobic modifications of colloidal silica particles for Pickering emulsions, J. Colloid Interface Sci. 487 (2017) 250–257, https://doi.org/10.1016/j.jcis.2016.10.031.
[33] N. Wang, Y. Luo, T. Liu, S. Qi, Y. Xu, M. Ma, H. Chen, P. Zhou, Mesoporous silica nanoparticles-reinforced hydrogel scaffold together with pinacidil loading to improve stem cell adhesion, ChemNanoMat 4 (2018) 631–641, https://doi.org/10.1002/cnma.201800026.
[34] W. Stöber, A. Fink, Controlled growth of monodisperse silica spheres in the micron size range, J. Colloid Interface Sci. 26 (1968) 62–69, https://doi.org/10.1109/ICOSP.2006.345929.
[35] D. González-Álvarez, R.J. Naranjo-Rodríguez, I. Hernández-Artiga, M.P. Palacios-Santander, J.M. Cubillana-Aguilera, L., & Bellido-Milla, Experimental design applied to optimisation of silica nanoparticles size obtained by sonosynthesis, J. Solgel Sci. Technol. 80 (2016) 378–388, https://doi.org/10.1007/s10971-016-4129-6.
[36] G. Giovannini, F. Kunc, C.C. Piras, O. Stranik, A.A. Edwards, A.J. Hall, V. Gubala, Stabilizing silica nanoparticles in hydrogels: impact on storage and polydispersity, RSC Adv. 7 (2017) 19924–19933, https://doi.org/10.1039/C7RA02427D.
[37] G. Chen, Z. Teng, X. Su, Y. Liu, G. Lu, Unique biological degradation behavior of stöber mesoporous silica nanoparticles from their interiors to their exteriors, J. Biomed. Nanotechnol. 11 (2015) 722–729, https://doi.org/10.1166/jbn.2015.2072.
[38] S.S. Park, C. Ha, Organic-inorganic hybrid mesoporous silicas: functionalization, pore size, and morphology control, Chem. Rec. 6 (2006) 32–42, https://doi.org/10.1002/tcr.20070.
[39] Z. Xu, X. Ma, Y.E. Gao, M. Hou, P. Xue, C.M. Li, Y. Kang, Multifunctional silica nanoparticles as a promising theranostic platform for biomedical applications, Mater. Chem. Front 1 (2017) 1257–1272, https://doi.org/10.1039/c7qm00153c.
[40] R.S. Fernandes, I.M. Raimundo, M.F. Pimentel, Revising the synthesis of Stöber silica nanoparticles: a multivariate assessment study on the effects of reaction parameters on the particle size, Colloids Surf. A Physicochem Eng. Asp. 577 (2019) 1–7, https://doi.org/10.1016/j.colsurfa.2019.05.053.
[41] X. Guillory, A. Tessier, G.O. Gratien, P. Weiss, S. Colliec-Jouault, D. Dubreuil, J. Lebreton, J. le Bideau, Glycidyl alkoxysilane reactivities towards simple nucleophiles in organic media for improved molecular structure definition in hybrid materials, RSC Adv. 6 (2016) 74087–74099, https://doi.org/10.1039/c6ra01658h.
[42] M. Nouri-Felekori, M. Khakbiz, N. Nezafati, J. Mohammadi, M.B. Eslaminejad, Comparative analysis and properties evaluation of gelatin microspheres crosslinked with glutaraldehyde and 3-glycidoxypropyltrimethoxysilane as drug delivery systems for the antibiotic vancomycin, Int J. Pharm. 557 (2019) 208–220, https://doi.org/10.1016/j.ijpharm.2018.12.054.
[43] L. Gabrielli, L. Russo, A. Poveda, J.R. Jones, F. Nicotra, J. Jiménez-Barbero, L. Cipolla, Epoxide opening versus silica condensation during sol-gel hybrid biomaterial synthesis, Chem. - A Eur. J. 19 (2013) 7856–7864, https://doi.org/10.1002/chem.201204326.
[44] Y. Shirosaki, K. Tsuru, S. Hayakawa, A. Osaka, M.A. Lopes, J.D. Santos, M. H. Fernandes, In vitro cytocompatibility of MG63 cells on chitosan-organosiloxane hybrid membranes, Biomaterials 26 (2005) 485–493, https://doi.org/10.1016/j.biomaterials.2004.02.056.
[45] G. Fernandez-Lorente, F. Lopez-Gallego, J.M. Bolivar, J. Rocha-Martin, S. Moreno-Perez, J.M. Guisan, Immobilization of proteins on glyoxyl activated supports: dramatic stabilization of enzymes by multipoint covalent attachment on pre-existing supports, Curr. Org. Chem. 19 (2015) 1–13, https://doi.org/10.2174/1385272819666150429232725.
[46] O. Chaudhuri, L. Gu, D. Klumpers, M. Darnell, A. Sidi, J.C. Weaver, N. Huebsch, H. Lee, E. Lippens, G.N. Duda, D.J. Mooney, Hydrogels with tunable stress relaxation regulate stem cell fate and activity, Nat. Mater. 15 (2016) 326–334, https://doi.org/10.1038/nmat4489.Hydrogels.
[47] M. Mostakhdemin, A. Nand, M. Ramezani, A novel assessment of microstructural and mechanical behaviour of bilayer silica-reinforced nanocomposite hydrogels as a candidate for artificial cartilage, J. Mech. Behav. Biomed. Mater. 116 (2021), 104333, https://doi.org/10.1016/j.jmbbm.2021.104333.
[48] V. Urbonaite, H.H.J. de Jongh, E. van der Linden, L. Pouvreau, Water holding of soy protein gels is set by coarseness, modulated by calcium binding, rather than gel stiffness, Food Hydrocoll. 46 (2015) 103–111, https://doi.org/10.1016/j.foodhyd.2014.12.010.
[49] F. Sani, F. Mehdipour, T. Talaei-Khozani, M. Sani, V. Razban, Fabrication of platelet-rich plasma/silica scaffolds for bone tissue engineering, Bioinspired, Biomim. Nanobiomaterials 7 (2017) 74–81, https://doi.org/10.1680/jbibn.17.00007.
[50] M. Arjmandi, M. Ramezani, Mechanical and tribological assessment of silica nanoparticle-alginate-polyacrylamide nanocomposite hydrogels as a cartilage replacement, J. Mech. Behav. Biomed. Mater. 95 (2019) 196–204, https://doi.org/10.1016/j.jmbbm.2019.04.020.
[51] S.N. Jayash, P.R. Cooper, R.M. Shelton, S.A. Kuehne, G. Poologasundarampillai, Novel chitosan-silica hybrid hydrogels for cell encapsulation and drug delivery, Int J. Mol. Sci. 22 (2021) 12267, https://doi.org/10.3390/ijms222212267.
[52] M. Danaei, M. Dehghankhold, S. Ataei, F. Hasanzadeh Davarani, R. Javanmard, A. Dokhani, S. Khorasani, M.R. Mozafari, Impact of particle size and polydispersity index on the clinical applications of lipidic nanocarrier systems, Pharmaceutics 10 (2018) 57, https://doi.org/10.3390/pharmaceutics10020057.
[53] A.J. Worthen, V. Tran, K.A. Cornell, T.M. Truskett, K.P. Johnston, Steric stabilization of nanoparticles with grafted low molecular weight ligands in highly concentrated brines including divalent ions, Soft Matter 12 (2016) 2025–2039, https://doi.org/10.1039/c5sm02787j.
[54] C. Gaviria, N.Y. Becerra, J.D. Vergara, L.A. Correa, S. Estrada, L.M. Restrepo, Dermo-epidermal organotypic cultures for in vitro evaluation of skin irritation and corrosion, Toxicol. Vitr. 63 (2020), 104657, https://doi.org/10.1016/j.tiv.2019.104657.
[55] P.K. Sharma, H.J. Busscher, T. Terwee, S.A. Koopmans, T.G. van Kooten, A comparative study on the viscoelastic properties of human and animal lenses, Exp. Eye Res 93 (2011) 681–688, https://doi.org/10.1016/j.exer.2011.08.009.
[56] R.H.J. de Hilster, P.K. Sharma, M.R. Jonker, E.S. White, E.A. Gercama, M. Roobeek, W. Timens, M.C. Harmsen, M.N. Hylkema, J.K. Burgess, Human lung extracellular matrix hydrogels resemble the stiffness and viscoelasticity of native lung tissue, Am. J. Physiol. Lung Cell Mol. Physiol. 318 (2020) L698–L704, https://doi.org/10.1152/AJPLUNG.00451.2019.
[57] F.D. Martinez-Garcia, R.H.J. de Hilster, P.K. Sharma, T. Borghuis, M.N. Hylkema, J. K. Burgess, M.C. Harmsen, Architecture and composition dictate viscoelastic properties of organ-derived extracellular matrix hydrogels, Polym. (Basel) 13 (2021) 3113, https://doi.org/10.3390/polym13183113.
[58] M. Nizamoglu, R.H.J. de Hilster, F. Zhao, P.K. Sharma, T. Borghuis, M.C. Harmsen, J.K. Burgess, An in vitro model of fibrosis using crosslinked native extracellular matrix-derived hydrogels to modulate biomechanics without changing composition, Acta Biomater. 147 (2022) 50–62, https://doi.org/10.1016/j.actbio.2022.05.031.
[59] X.S. Zhao, G.Q. Lu, A.K. Whittaker, G.J. Millar, H.Y. Zhu, Comprehensive study of surface chemistry of MCM-41 using 29Si CP/MAS NMR, FTIR, pyridine-TPD, and TGA, J. Phys. Chem. B 101 (1997) 6525–6531, https://doi.org/10.1021/jp971366.
[60] M. Templin, U. Wiesner, H.W. Spiess, Multinuclear solid-state-NMR studies of hybrid organic-inorganic materials, Adv. Mater. 9 (1997) 814–817, https://doi.org/10.1002/adma.19970091011.
[61] E.P.F. Nhavene, W.M. da Silva, R.R. Trivelato Junior, P.L. Gastelois, T. Venâncio, R. Nascimento, R.J.C. Batista, C.R. Machado, W.A. de A. Macedo, E.M.B. de Sousa, Chitosan grafted into mesoporous silica nanoparticles as benznidazol carrier for Chagas diseases treatment, Microporous Mesoporous Mater. 272 (2018) 265–275, https://doi.org/10.1016/j.micromeso.2018.06.035.
[62] J. Diosa, J.C. Poveda-Jaramillo, F. Ramirez-Rodríguez, M. Mesa, Modeling surface chemistry and adsorption behavior of biomimetic chitosan/silica hybrid materials,

J. Mater. Res. Technol. 9 (2020) 8092–8103, https://doi.org/10.1016/j.jmrt.2020.05.100.
[63] C. Tang, J. Zhu, Q. Zhou, J. Wei, R. Zhu, H. He, Surface heterogeneity of SiO2 polymorphs: an XPS investigation of α-quartz and α-cristobalite, J. Phys. Chem. C. 118 (2014) 26249–26257, https://doi.org/10.1021/jp509338x.
[64] S. Jafari Daghlian Sofla, L.A. James, Y. Zhang, Insight into the stability of hydrophilic silica nanoparticles in seawater for Enhanced oil recovery implications, Fuel 216 (2018) 559–571, https://doi.org/10.1016/j.fuel.2017.11.091.
[65] P. Innocenzi, C. Figus, T. Kidchob, M. Valentini, B. Alonso, M. Takahashi, Sol-gel reactions of 3-glycidoxypropyltrimethoxysilane in a highly basic aqueous solution, Dalton Trans. 9 (2009) 9146–9152, https://doi.org/10.1039/b905830c.
[66] M. Arjmandi, M. Ramezani, Mechanical and tribological assessment of silica nanoparticle-alginate- polyacrylamide nanocomposite hydrogels as a cartilage replacement, J. Mech. Behav. Biomed. Mater. 95 (2019) 196–204, https://doi.org/10.1016/j.jmbbm.2019.04.020.
[67] W.C. Huang, T.J. Lee, C.S. Hsiao, S.Y. Chen, D.M. Liu, Characterization and drug release behavior of chip-like amphiphilic chitosan-silica hybrid hydrogel for electrically modulated release of ethosuximide: an in vitro study, J. Mater. Chem. 21 (2011) 16077–16085, https://doi.org/10.1039/c1jm12376a.
[68] C. Karavasili, K. Tsongas, I.I. Andreadis, E.G. Andriotis, E.T. Papachristou, R. M. Papi, D. Tzetzis, D.G. Fatouros, Physico-mechanical and finite element analysis evaluation of 3D printable alginate-methylcellulose inks for wound healing applications, Carbohydr. Polym. 247 (2020), 116666, https://doi.org/10.1016/j.carbpol.2020.116666.
[69] Y. Wang, F. Zhu, Q. Rao, X. Peng, A 3D finite strain viscoelastic model with uncoupled structural and stress relaxations for shape memory polymers, Polym. Test. 103 (2021), 107373, https://doi.org/10.1016/j.polymertesting.2021.107373.
[70] M.I.P. Vargas, F.D. Martinez-Garcia, F. Offens, N.Y. Becerra, L.M. Restrepo, H. C. van der Mei, M.C. Harmsen, T.G. van Kooten, P.K. Sharma, Viscoelastic properties of plasma-agarose hydrogels dictate favorable fibroblast responses for skin tissue engineering applications, Biomater. Adv. 139 (2022), 212967, https://doi.org/10.1016/j.bioadv.2022.212967.